Modeling of the flow-solidification interaction in thin slab casting

2012 IOP Conf. Ser.: Mater. Sci. Eng. 33 012014

(http://iopscience.iop.org/1757-899X/33/1/012014)

Modeling of the flow-solidification interaction in thin slab casting

A Vakhrushev[1], **M Wu**[1,2], **A Ludwig**[2], **Y Tang**[3], **G Hackl**[3], **G Nitzl**[4]
[1]Christian-Doppler Lab for Adv. Process Simulation of Solidification & Melting,
[2]Chair of Simulation & Modelling of Metallurgical Processes,
University of Leoben, Franz-Josef-Str. 18, 8700 Leoben, Austria
[3]RHI AG, Technology Center, Magnesitstrasse 2, 8700 Leoben, Austria
[4]RHI AG, Wienerbergstrasse 9, 1100 Vienna, Austria

E-mail: alexander.vakhrushev@unileoben.ac.at

Abstract. A key issue for modelling the thin slab casting (TSC) is to consider the evolution of the solid shell, which strongly interacts with the turbulent flow and in the meantime is subject to continuous deformation due to the funnel shape (curvature) of the mould. Here an enthalpy-based mixture solidification model with consideration of turbulent flow [Prescott and Incropera, *ASME HTD*, vol. 280, 1994, pp. 59] is employed, and further enhanced to include the deforming solid shell. The solid velocity in the fully-solidified strand shell and partially-solidified mushy zone is estimated by solving the Laplace's equation. Primary goals of this work are to examine the sensitivity of the modelling result to different model implementation schemes, and to explore the importance of the deforming and moving solid shell in the solidification. Therefore, a 2D benchmark, to mimic the solidification and deformation behaviour of the thin slab casting, is firstly simulated and evaluated. An example of 3D TSC is also presented. Due to the limitation of the current computation resources additional numerical techniques like parallel computing and mesh adaptation are necessarily applied to ensure the calculation accuracy for the full-3D TSC.

1. Introduction

The thin slab casting (TSC), for its advantages of integration of the casting-rolling production chain, energy saving, high productivity and near net shape, is likely to replace the conventional slab casting for producing flat/strip products [1-2]. However, the frequently reported problems like the sensibility to breakout and edge/surface cracks have challenged the metallurgists to consider modeling tools to optimize and control the TSC parameters [3-5]. The key issue for modelling TSC is to consider the evolution of the solid shell, which interacts strongly with the turbulent flow and in the meantime is subject to continuous deformation due to the funnel shape (curvature) of the mould.

An enthalpy-based mixture solidification model with consideration of turbulent flow [6-9] was introduced by the current authors to model conventional continuous casting [10-11], where the motion of the solid shell was assumed to be everywhere parallel and constant. According to Voller et al., the treatment of the motion of the solid phase has a dramatic influence on the convection of the latent heat, hence on the shape of the evolving mushy zone [12-15]. Obviously, the assumption of parallel-constant solid velocity does not apply to TSC, where the strand shell is subject to continuous deformation due to the funnel shape (curvature) of the mould. Therefore, goals of this work are (1) to extend the previous model by considering the deforming solid shell; (2) to examine the sensitivity of

the modelling result to different model implementation schemes; (3) and to explore the importance of the deforming and moving solid shell in the solidification. Modelling results on a 2D benchmark and a full-3D TSC are presented.

2. Model description

Solidification and turbulence flow

An enthalpy-based mixture solidification model [12-14] is applied. This mixture combines liquid ℓ-phase and solid s-phase, which are quantified by their volume fractions, f_ℓ and f_s. The morphology of the solid phase is usually dendritic, but here we consider the dendritic solid phase as a part of the mixture continuum. The mixture continuum changes continuously from a pure liquid region, through the mushy zone (two phase region), to the complete solid region. The evolution of the solid phase is determined by the temperature according to a $f_s - T$ relation (e.g. Gulliver-Scheil),

$$f_s = \begin{cases} 0 & T > T_{\text{liquidus}} \\ 1 - \left((T_{\text{f}} - T)/(T_{\text{f}} - T_{\text{liquidus}})\right)^{\frac{1}{k_{\text{p}}-1}} & T_{\text{liquidus}} \geq T > T_{\text{Eutectic}} \\ 1 & T_{\text{Eutectic}} \leq T. \end{cases} \quad (1)$$

Only one set of Navier-Stokes equation, which applies only to the domain of the bulk melt and mushy zone, is solved in the Eulerian frame of reference.

$$\nabla \cdot \vec{u} = 0, \quad (2)$$

$$\rho \frac{\partial \vec{u}}{\partial t} + \rho \nabla \cdot (\vec{u} \otimes \vec{u}) = -\nabla p + \nabla(\mu_{\text{eff}} \nabla \cdot \vec{u}) + \vec{S}_{\text{mon}}, \quad (3)$$

$$\text{where } \vec{u} = \begin{cases} \vec{u}_\ell & \text{bulk melt region} \\ f_\ell \vec{u}_\ell + f_{\text{s}} \vec{u}_{\text{s}} & \text{mushy zone} \\ \vec{u}_{\text{s}} & \text{solid region.} \end{cases} \quad (4)$$

Here $\vec{u}_{\text{s}}$, the solid velocity, is estimated by solving Laplace's equations (see below). The momentum sink due to the drag of the solid dendrites in the mushy zone is modeled by the Blake-Kozeny law:

$$\vec{S}_{\text{mon}} = -\frac{\mu_\ell}{K} \cdot (\vec{u} - \vec{u}_{\text{s}}) \quad (5)$$

The permeability, *K*, is modeled as function of the primary dendrite arm spacing λ_1 [16]:

$$K = \frac{f_\ell^{\,3}}{f_{\text{s}}^{\,2}} \cdot 6 \cdot 10^{-4} \cdot \lambda_1^2. \quad (6)$$

The energy equation applies to the entire domain,

$$\rho \frac{\partial h}{\partial t} + \rho \nabla \cdot (\vec{u} h) = \nabla \cdot \lambda_{\text{eff}} \nabla T + S_{\text{e}}. \quad (7)$$

Here h is the sensible enthalpy of the solid $h_{\text{s}} = h_{\text{ref}} + \int_{T_{\text{ref}}}^{T} c_{\text{p}} dT$. At a given temperature the liquid phase is assumed to have an enthalpy of $h_\ell = h_{\text{s}} + L$. Release of latent heat by solidification, *L*, is treated in the source term of the energy equation,

$$S_{\text{e}} = \rho L \, \partial f_{\text{s}} / \partial t + \rho L \nabla \cdot (f_{\text{s}} \vec{u}_{\text{s}}). \quad (8)$$

A low Reynolds number k-ε model was introduced by Prescott and Incropera [6-9] to handle the turbulence during solidification. In current studies a realizable k-ε model was employed providing improved performance for flows involving boundary layers under strong pressure gradients and strong streamline curvature. The governing equations for the turbulence are

$$\frac{\partial(\rho k)}{\partial t}+\nabla\cdot(\rho\vec{u}k)=\nabla\cdot\left(\left(\mu_\ell+\frac{\mu_t}{\mathrm{Pr}_{t,k}}\right)\nabla k\right)+G-\rho\varepsilon-\frac{\mu_\ell}{K}\cdot k\,, \tag{9}$$

$$\frac{\partial(\rho\varepsilon)}{\partial t}+\nabla\cdot(\rho\vec{u}\varepsilon)=\nabla\cdot\left(\left(\mu_\ell+\frac{\mu_t}{\mathrm{Pr}_{t,\varepsilon}}\right)\nabla\varepsilon\right)+\rho C_{1\varepsilon}S\varepsilon-C_{2\varepsilon}\rho\frac{\varepsilon^2}{k+\sqrt{\nu\varepsilon}}\,. \tag{10}$$

The turbulent Prandtl numbers for k : $\mathrm{Pr}_{t,k}$=1.0, and for ε : $\mathrm{Pr}_{t,\varepsilon}$=1.2; G is the shear production of turbulence kinetic energy; $S=\sqrt{2S_{ij}S_{ij}}$, $S_{ij}=0.5(\partial u_j/\partial x_i+\partial u_i/\partial x_j)$; $\nu=S\cdot k/\varepsilon$. A simple approach is used to modify the turbulence kinetic energy in the mushy zone. It is assumed that within a coherent mushy zone turbulence is dampened by shear which is linearly correlated with the reduction of the mush permeability. The influence of turbulence on the momentum and energy transports are considered by the effective viscosity, $\mu_{\mathrm{eff}}=\mu_\ell+\mu_t$, and the effective thermal conductivity, $\lambda_{\mathrm{eff}}=\lambda_\ell+\lambda_t$, where $\mu_t=\rho C_\mu k^2/\varepsilon$, $\lambda_t=f_\ell\mu_t c_{p,\ell}/\mathrm{Pr}_{t,h}$, C_μ is a function of velocity gradient and ensures positivity of normal stresses; $\mathrm{Pr}_{t,h}$ is the turbulent Prandtl number for energy equation (0.85).

Above governing equations of the mixture solidification model were implemented in an OpenFOAM® CFD software package [17-18].

Solid velocity

A linear elasticity model [19] is further simplified to estimate the solid velocity. If we assume that in the solid domain the elastostatics condition applies and the body force is ignorable, the governing equation obtained is called Navier-Cauchy equation or elastostatic equation:

$$(\lambda+\mu)\,\nabla(\nabla\cdot\vec{\delta})+\mu\,\nabla\cdot\nabla\vec{\delta}=0\,, \tag{11}$$

where $\vec{\delta}$ is the displacement vector. So called Lamé parameters λ, μ are

$$\lambda=\frac{E\nu}{(1+\nu)(1-2\nu)},\quad \mu=\frac{E}{2(1+\nu)}, \tag{12}$$

where E represents Young's modulus and ν is Poisson's ratio. If the solid shell is incompressible and its deformation is at small strains ($\nu=0.5$), then a volume conservation condition is fulfilled:

$$\nabla\cdot\vec{\delta}=0\,, \tag{13}$$

and the first term of Eq. (11) is forced to zero as well:

$$\nabla\cdot\nabla\vec{\delta}=0\,. \tag{14}$$

Transforming Eq.(13) and (14) from Lagragian frame into Eulerian frame by considering $\vec{u}_s=\partial\vec{\delta}/\partial t$, we obtain volume-conserved Laplace's equations:

$$\begin{cases}\nabla\cdot\nabla\vec{u}_s=0,\\ \nabla\cdot\vec{u}_s=0.\end{cases} \tag{15}$$

In 2D case, these volume-conserved Laplace's equations can be solved with a $\omega-\psi$ method (Method I) [20]. A stream function ψ and a curl of the solid velocity $\omega=\nabla\times\vec{u}_s$ are defined by:

$$u_s^x = \frac{\partial \psi}{\partial y}, \quad u_s^y = -\frac{\partial \psi}{\partial x}, \quad \omega = \frac{\partial u_s^y}{\partial x} - \frac{\partial u_s^x}{\partial y}, \tag{16}$$

with $\vec{u}_s = (u_s^x, u_s^y)^T$. Therefore, corresponding system of Eq. (15) can be written in form of:

$$\begin{cases} \dfrac{\partial^2 \psi}{\partial x^2} + \dfrac{\partial^2 \psi}{\partial y^2} = -\omega, \\ \dfrac{\partial^2 \omega}{\partial x^2} + \dfrac{\partial^2 \omega}{\partial y^2} = 0. \end{cases} \tag{17}$$

This $\omega - \psi$ method provides accurate solution, but it applies only to the 2D case. An alternative and approximation method (Method II), applicable to both 2D and 3D, is to solve the one-phase Navier-Stokes equation with an 'infinite solid viscosity'. In the current work the approximation method is to be justified by comparison with the $\omega - \psi$ method on the 2D base.

3. Benchmark (2D) configuration

A 2D benchmark is defined, as shown in Figure 1. The melt with nominal composition of Fe-0.34wt.%C fills continuously through the inlet into the domain with constant temperature (1850 K). The casting section is gradually reduced to mimic the solidification and shell deformation in TSC. Other material properties being used refer to [11]. Solid velocity is calculated with the configuration of Figure 1(a). The whole domain is filled with the solid which is extruded downwards with the constant speed $\vec{u}_{\text{pull}}$=0.07 m/s, being set at the outlet. Free slip condition is applied at the walls and non-rotational condition ($\nabla \times \vec{u}_s = 0$) is used at the inlet. Right boundary represents symmetry plane. Flow-solidification simulation is configured in Figure 1(b). A mass balance between the inlet and the outlet is fulfilled: $\rho_\ell \vec{u}_{\text{in}} A_{\text{in}} = \rho_s \vec{u}_{\text{pull}} A_{\text{out}}$, where A_{in} and A_{out} are the inlet and outlet surface areas. At the walls free-slip condition is assumed.

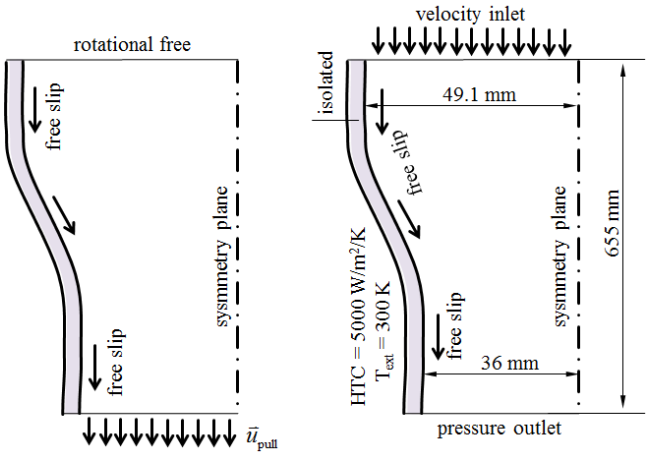

Figure 1. Configuration of a 2D benchmark (a) for solid velocity calculation and (b) for the solidification–flow calculation. The geometry in vertical direction is scaled by 1/8 (the same hereafter).

4. Results and discussions

In the presented studies solid velocities calculation is decoupled from the simulation of the melt flow. They are initially estimated by solving (15) with an assumption that the whole domain is filled with the solid and are used later on for the solidification modeling in the mush region only. Thereby liquid core in the center can accelerate or retard for balancing the total mass flow rate. The calculated solid velocity, $\vec{u}_s$, is shown in Figure 2 (a)-(b). Solid phase enters the domain in parallel to the straight wall. In the section-reduction region the solid is extruded and its velocity is gradually increased. The surface profile is forced to move along the curved wall. Comparison of the calculation results by two different methods (I and II) is made in Figure 2(b)-(d). The

maximum error caused by method II, solving a simplified Navier-Stokes equation with an 'infinite solid viscosity', is 0.8%, falling in the engineering tolerance. This solid velocity will only be used by the flow-solidification model, Eq.(5) and (8), in the region where solid phase exists.

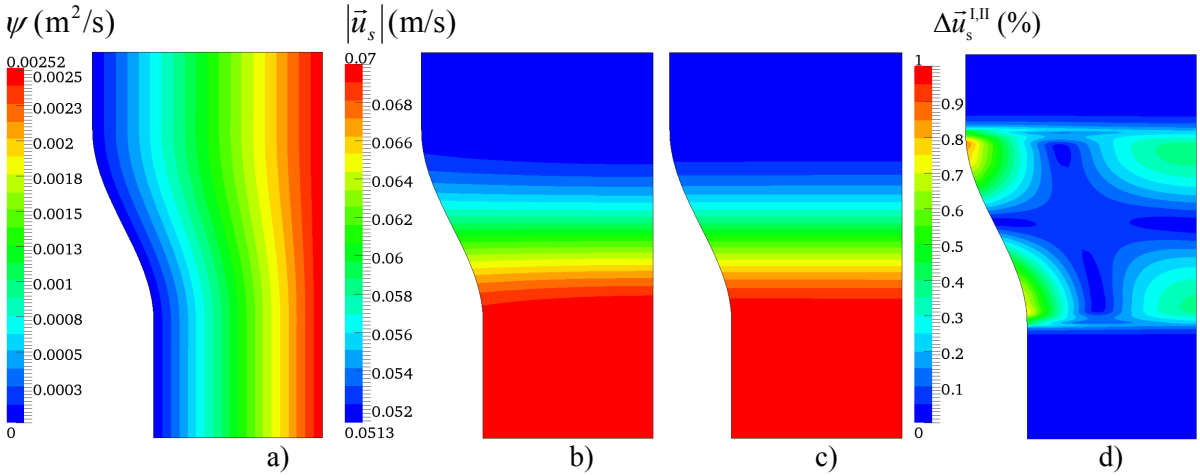

Figure 2. Calculated solid velocity: (a) stream function ψ, (b) $|\vec{u}_s|$ obtained with $\omega-\psi$ Method I, (c) $|\vec{u}_s|$ obtained with 'infinite solid viscosity' Method II and (d) velocity difference between the two methods ($\Delta\vec{u}_s^{\,I,II} = \left|\vec{u}_s^{\,I} - \vec{u}_s^{\,II}\right| / \left|\vec{u}_s^{\,I}\right| \cdot 100$).

Table 1. Parameter study of the flow-solidification model

	Flow regime	Treatment of latent heat (Eq.(8))	f_s^{integral} (vol.%)*
Case I	laminar	S_e	9.38
Case II	laminar	ignoring $\rho L\nabla\cdot(f_s\vec{u}_s)$ in S_e	15.34
Case III	turbulent	S_e	8.81
Case IV	turbulent	ignoring $\rho L\nabla\cdot(f_s\vec{u}_s)$ in S_e	14.04

* f_s^{integral} : total solid phase (vol.%) in the whole calculation domain at the steady state.

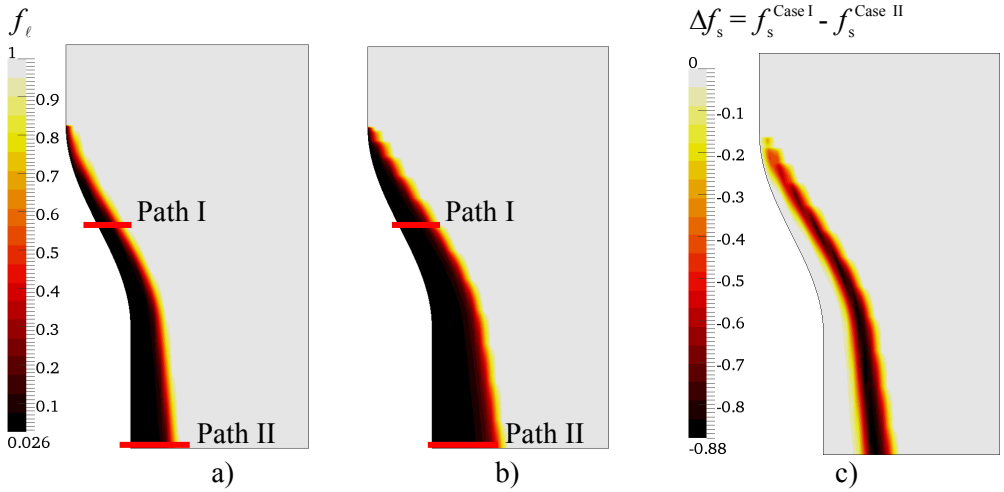

Figure 3. Predicted steady state solidification with a model considering only laminar flow: f_ℓ distribution for (a) Case I and (b) Case II; (c) difference in f_s between Case I and Case II.

In order to investigate different model assumptions, e.g. the influence of solid velocity and turbulence, on the solid shell formation by solidification, 4 simulation cases are defined (Table 1). For the boundary conditions refer to Figure 1(b). The predicted solid shell formation for the Case I and II (only laminar flow is considered) at the steady state is shown in Figure 3. Obviously the treatment of the advection of latent in the energy equation is extremely important. Ignorance of the advection term, $\rho L\nabla\cdot\left(f_s\bar{u}_s\right)$, in Case II will to a great extent overestimate the solid shell thickness. More precise analyses of the solid phase distributions along Path I and II, marked in Figure 3(a) and (b), are made in Figure 4.

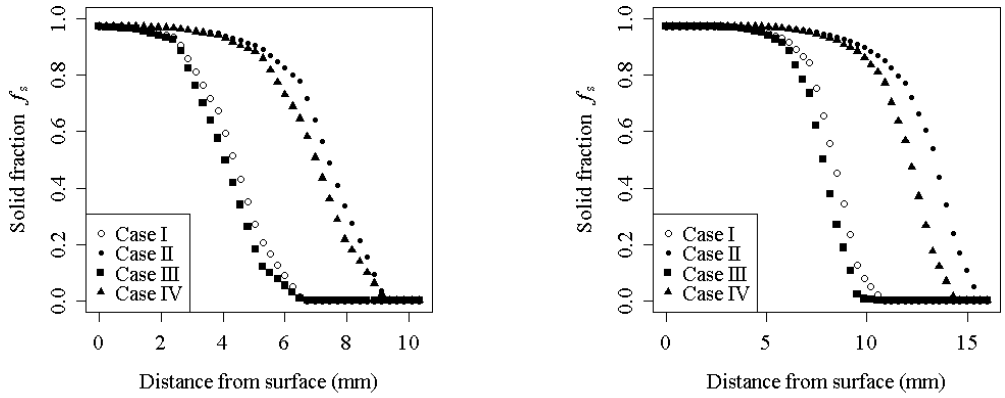

Figure 4. Solid volume fraction distributions of different simulation cases along (a) Path I and (b) Path II are compared.

Similar calculations were carried out for the turbulent flow regime, but are not displayed here because the global phase distribution shows similar pattern to the Case I and II. Instead the influence of the turbulence on the solid shell formation is analysed (Figure 5). Comparison between Cases III and I shows that the presence of turbulence hinders the solid shell formation. Ignorance of the advection term, $\rho L\nabla\cdot\left(f_s\bar{u}_s\right)$, will also overestimate the solid shell thickness. More precise analyses of the solid phase distributions alone two Path I and II, marked in Figure 3(a) and (b), for the simulation Cases III and IV are also made in Figure 4.

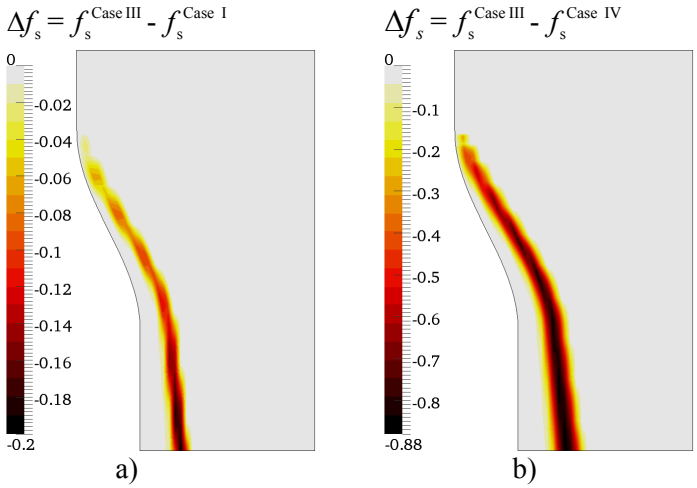

Figure 5. Influence of turbulence on the solid shell formation, i.e. the difference in f_s distribution (a) between Cases III and I, (b) between Cases III and IV.

Additionally a mesh and time step dependency of the numerical solution was examined. A low latent heat relaxation factor (0.05) [11] along with a relatively large number of iterations (50 per time-step) allowed using a relatively large time steps without problem of divergence. It was shown that the increase in time step did not influence the final steady state solution. To improve the accuracy a necessity to use separate refinement regions for the temperature and solid fraction fields was approved previously by authors [21]. Thereby based on the error analysis of the energy equation and the resolution criterion of the Gulliver-Scheil correlation (Eq.(1)), consecutive mesh refinements were made (Figure 6). Eventually mesh independent results were obtained.

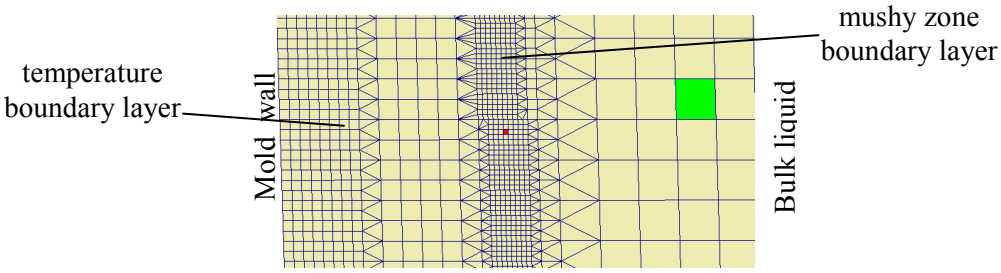

Figure 6. Mesh refinement to track the temperature boundary layer and solidification front

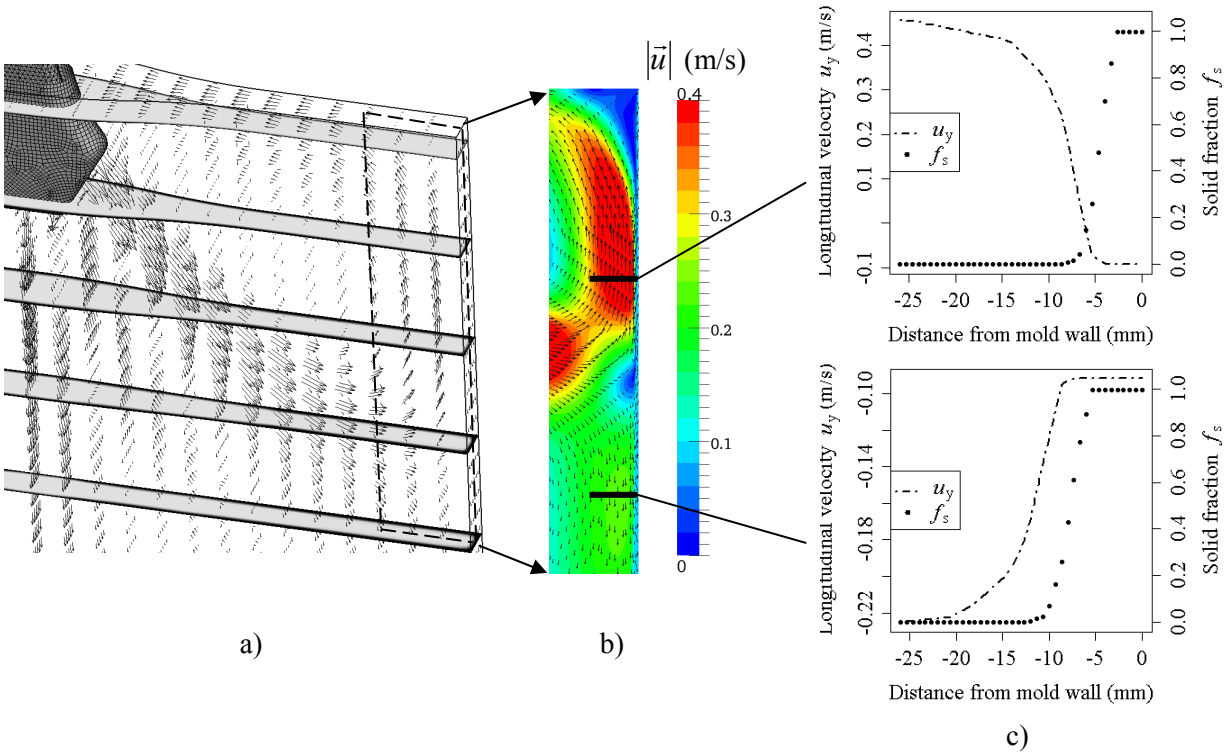

Figure 7. Quasi steady state simulation result of an engineering TSC. a) 3D distribution of the velocity vector field and evolution of the solid shell (dark region in the 5 cross sections); b) zoomed velocity field in the central plane near the narrow face; c) detailed velocity (u_y component) profile and solid volume fraction along two paths cross the mushy zone.

5. Example of thin slab casting

Based on the aforementioned model a simulation of the real engineering TSC (width 1726 mm and thickness 72 mm) was performed, and the calculation result is shown in Figure 7. The calculation domain includes the submerge entry nozzle and entire mold region and part of water cooled strand (till 2000 mm from meniscus). To ensure the calculation accuracy numerical techniques like parallel

computing and mesh adaptation are necessarily applied. More than 1 million computational cells are used to resolve the interdendritic flow in the mushy zone (Figure 7(c)). In [17,18] Laplace's equation was solved for solid velocities with a constant vertical component assumption restricting longitudinal deformations. The new approach doesn't have such a limitation and helps to mimic the mush better. Detailed analysis of the 3D simulation result and evaluation will be presented in later publication.

6. Summary

Combination of flow-solidification calculation with the deforming solid shell, oriented to the application in thin slab castings, is suggested. The numerical model is implemented in an OpenFOAM® CFD open source software package. As no additional structure mechanics software is used, the motion of the solid shell is estimated on the base of a volume-conserved Laplace's equations. Validity of the proposed approach is verified in a 2D benchmark. Preliminary modelling result of a 3D thin slab casting is also presented to demonstrate the functionality of the numerical model. Further verifications, especially against experiments, are desired.

Acknowledgment

The financial support by RHI AG, the Austrian Federal Ministry of Economy, Family and Youth and the National Foundation for Research, Technology and Development is gratefully acknowledged. The authors acknowledge the fruitful discussions with Prof. Brian G. Thomas, University of Illinois at Urbana-Champaign, USA.

References

[1] Yin RY 2009 *J. Iron & Steel Res.* **16** (Supplement 1) 1.
[2] Birat JP and Bobadilla M 2006 *Proc. McWASP XI* (Eds: Gandin CA and Bellet M, TMS Publications) 33.
[3] Tang Y, Krobath M, Nitzl G, Eglsaeer C and Morales R 2009 *J. Iron & Steel Res.* **16** (Supplement 1) 173.
[4] Thomas BG 2001 *Brimacombe Lecture, 59th Electric Furnace Conf.* (Iron & Steel Soc.) 3.
[5] Tian X, Zou F, Li B and He J 2010 *Metall. Mater. Trans.* **41B** 112.
[6] Prescott PJ and Incropera FP 1994 *Transp. Phen. in Mater. Proc. & Manuf.- ASME HTD* **280** 59.
[7] Prescott PJ and Incropera FP 1994 *J. Heat Transfer* **116** 735.
[8] Prescott PJ, Incropera FP and Gaskell DR 1994 *Trans. ASME* **116** 742.
[9] Prescott PJ and Incropera FP 1995 *Trans. ASME* **117** 716.
[10] Pfeiler C, Thomas BG, Wu M, Ludwig A and Kharicha A 2008 *Steel Res. Int.* **79** 599.
[11] Wu M, Vakhrushev A, Nummer G, Pfeiler C, Kharicha A and Ludwig A 2010 *Open Transport Phenomena J. – Bentham Open* **2** 16.
[12] Voller VR and Prakash C 1987 *Int. J. Heat Mass Transfer* **30** 1709.
[13] Voller VR, Brent AD and Prakash C 1989 *Int. J. Heat Mass Transfer* **32** 1719.
[14] Voller VR, Brent AD and Prakash C 1990 *Appl. Math. Modeling* **14** 320.
[15] Chakraborty PR and Dutta P 2011 *Metall. Mater. Trans.* **42B** in press (DOI: 10.1007/s11663-011-9585-3).
[16] Gu JP and Beckermann C 1999 *Metall. Mater. Trans.* **33A** 1357.
[17] Vakhrushev A, Ludwig A, Wu M, Tang Y, Nitzl G and Hackl G 2010 *Proc. OSCIC'10.* (Munich, Nov. 4-5).
[18] Vakhrushev A, Ludwig A, Wu M, Tang Y, Nitzl G and Hackl G 2011 *Proc. ECCC* (Düsseldorf, June 27 – July 01).
[19] Slaughter WS 2002 *The Linearized Theory of Elasticity* (Boston: Birkhäuser).
[20] Roache PJ 1998 *Fundamentals of Computational Fluid Dynamics* (New Mexico: Hermosa Publishers)
[21] Vakhrushev A, Ludwig A, Wu M, Tang Y, Nitzl G and Hackl G 2011 *Proc. OSCIC'11.* (Paris Chantilly, Nov. 3-4).